The Astrophysical Journal Letters, 712:L77–L80, 2010 March 20 doi:10.1088/2041-8205/712/1/L77

CORONAL MASS EJECTIONS AND SUNSPOTS—SOLAR CYCLE PERSPECTIVE

K. B. Ramesh
Indian Institute of Astrophysics, Koramangala, Bangalore 560034, India; kbramesh@iiap.res.in
Received 2010 January 8; accepted 2010 February 11; published 2010 March 3

ABSTRACT

Recent studies have indicated that the occurrence of the maxima of coronal mass ejection (CME) rate and sunspot number (SSN) were nearly two years apart. We find that the two-year lag of CME rate manifests only when the SSN index is considered and the lag is minimal (two–three months) when the sunspot area is considered. CMEs with speeds greater than the average speed follow the sunspot cycle much better than the entire population of CMEs. Analysis of the linear speeds of CMEs further indicates that during the descending phase of the solar cycle the loss of magnetic flux is through more frequent and less energetic CMEs. We emphasize that the magnetic field attaining the nonpotentiality that represents the free energy content, rather than the flux content as measured by the area of the active region, plays an important role in producing CMEs.

Key words: Sun: coronal mass ejections (CMEs) – sunspots

1. INTRODUCTION

Long-term variations in the occurrence rate of coronal mass ejections (CMEs) and associated physical parameters have been studied (Gopalswamy et al. 2004) in the recent past using LASCO CME data (Brueckner et al. 1995). Because solar rotation and the 11 year solar cycle modulate the evolution of magnetic flux of the Sun, different measures of solar activity normally are well correlated. CMEs bring about large-scale changes in the corona, which have fundamental implications for the evolution of the magnetic flux of the Sun that is ultimately related to the solar dynamo (Low 2001). Therefore, it is reasonable to expect a good correlation between the various properties of CMEs and the other tracers of solar activity such as sunspot number (SSN), type II radio bursts, and prominences. It is to be noted that the time evolution of different solar activity parameters, however, does not match exactly due to the complicated dynamics involved at different depths in the solar atmosphere (Kane 2006). One such difference is the mismatch in the peak occurrence of the halo CME rate and the SSN during solar cycle 23 (Gopalswamy et al. 2003). They have identified that the maximum CME rate occurred two years after the peak occurrence of SSN. In a recent study, it was pointed out that the sunspot areas (SAs) better represent the solar cycle than the SSN (Ramesh & Rohini 2008). In this context, we examine here the characteristics of CMEs with particular reference to their rate of occurrence and speeds in association with the SAs and SSN. Since the energetic and fast CMEs originate mostly from the solar active regions and the slow ones are associated with erupting prominences (Gosling et al. 1976; Sheeley et al. 1999; Gopalswamy et al. 2009), we felt it appropriate to use speeds of CMEs to bring out their relationship with the variability of the occurrences of sunspots.

2. SOURCES OF THE DATA

The number of CMEs per day and their speed information are taken from the CME catalogs at http://cdaw.gsfc.nasa.gov/CME_list and http://sidc.oma.be/cactus. SA and international SSN data are obtained from http://solarscience.msfc.nasa.gov/greenwch.shtml and ftp://ftp.ngdc.noaa.gov/STP/SOLAR_DATA/SUNSPOT_NUMBERS, respectively.

3. ANALYSIS AND DISCUSSION

Figure 1(a) shows the rate of occurrence (Rw) of CMEs averaged over each Carrington rotation (CR). CMEs with angular width less than 30° are excluded in the data presented in the figure because the manual detection of such CMEs is highly subjective (Yashiro et al. 2008). Cremades & St. Cyr (2007) have opined that all the CMEs have to be taken into account without any distinction of their width because even if wide CMEs are likely to have inherent projection effects attached, their speeds are nevertheless remarkably higher than for normal CMEs. Keeping both of these points in view, we discuss the solar cycle variability in the CME rate. Overplotted is a thin continuous line that represents the running means of CME rate averaged over 13 rotations. The cotemporal plot for SSN is shown in Figure 1(c). It is interesting to note that while the SSN profile shows an unmistakable double-humped pattern, such a feature is not discernible in the yearly running mean occurrence rate of CMEs (Figure 1(a)). The double-humped pattern, however, emerges when the entire population of CMEs is considered without any attention to their widths (Ra, thin line). Gopalswamy et al. (2003) have compared the double-humped pattern depicted by the CME rate with that of the pattern depicted by SSN. They have indicated that the peak occurrence of CME rate (during 2002) is delayed by about two years when compared to the one in SSN that peaked during the year 2000. Gopalswamy et al. (2009) have further analyzed CME occurrence in relation to SSN to show that the correlation between them seemed to be quite weak during the period of maximum phase of the solar cycle when compared to that in ascending as well as descending phases. They have identified the contribution of quiescent filament associated CMEs to their rate of occurrence as the cause of this reduced correlation.

Figure 1(b) depicts the rate (Rw) of occurrence of CMEs with linear speeds greater than the average speed (452 km s^{-1}). Overplotted is a thick continuous line representing the running means of Rw averaged over 13 rotations. All through the solar cycle, the CME rate seems to have decreased by a factor of 2 indicating the occurrence of low-speed CMEs without any preference to the phase of the solar cycle. The double-humped pattern is more pronounced with an unambiguous increased second peak. Similar pattern is repeated in the profile of CME rate (thin line) for the entire population of CMEs (Ra). In this

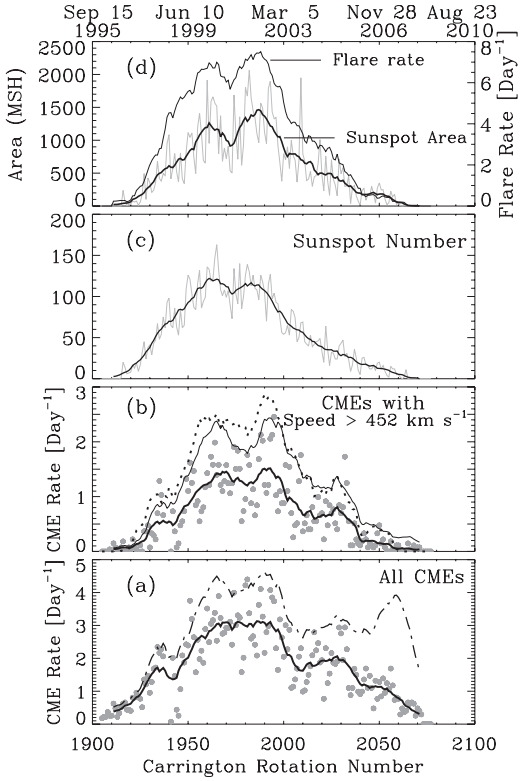

Figure 1. Solar cycle variation of the occurrence of CMEs. (a) Filled circles represent the CR averages of daily number of CMEs for the CMEs with widths greater than 30°. Overplotted thick continuous line is the 13 CR averages. Thin line is the same as that of thick continuous line but for the CMEs without any distinction to the width. (b) The same as that of (a) but for the CMEs with linear speeds greater than the average speed (452 km s^{-1}). Dotted curve represents the 13 rotation-smoothed CR averages of CMEs taken from CACTus catalog. CACTus CME rate suitably scaled to fit into the plot. (c) CR averages (gray) and 13 CR smoothed (thick) SSNs. (d) CR averages (gray) and 13 CR smoothed (thick) SAs (in millionths of the solar hemisphere, MSH). Flare rate is also shown for comparison. Note the larger second crest (compared to the first one) of the double-humped pattern in both (b) and (d), while in (c) it is opposite.

case the average speed is 426 km s^{-1}. The CME rate (dotted line) deduced from the CACTus (Computer Aided CME Tracking) catalog of CMEs (Robbrecht et al. 2009) also shows an increased second peak around CR 1990.

In a recent study, Ramesh & Rohini (2008) have shown that the SA represents well the solar cycle when compared to SSN and that the delay of about two years between X-ray background flux (XBF) and sunspot activity is a result of the underestimation of SSN caused by identical weights assigned to all spot groups. With this perspective, we have now examined the relation between the CME rate and the SAs. CR-averaged SA (gray line) is shown in Figure 1(d). Thirteen rotation-averaged SAs (thick line) overplotted on the CR-averaged SA show an unambiguous double-humped pattern during maximum phase of the cycle and that the dominant second peak occurred around CR 1990 in near coincidence with the second peak of CMEs as well as SSN. It is known that the CME and flare occurrence rates are related (Lippiello et al. 2008). The flare rate, for the flare importance greater than "C," shown in Figure 1(d) demonstrates amply the near coincidence of dominant second peak with that of SA and the CME rate (Figure 1(b)).

Figure 2(a) shows the plots of CME (with angular width greater than 30°) rate (Rw) for the entire population and randomly chosen lower cutoff speeds of 200, 452 (average speed), 500, 600, 800, and 1000 km s^{-1}. Figure 2(b) shows the plots of CME rate (Ra) for entire population without any

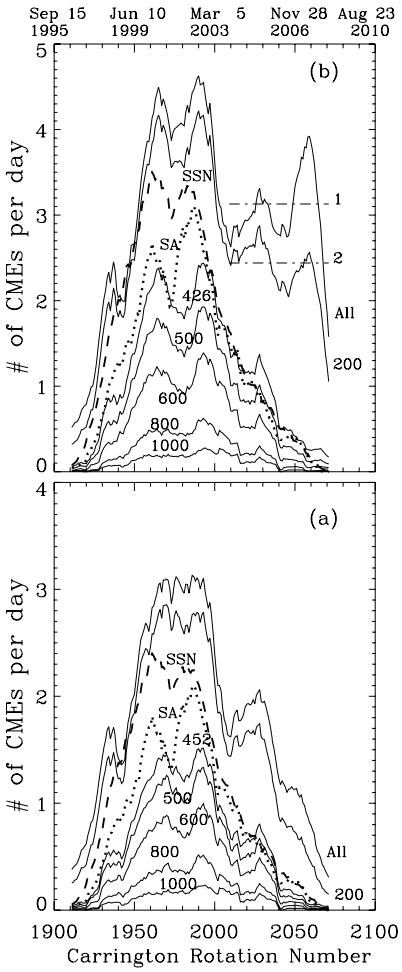

Figure 2. (a) Thin continuous lines represent the 13 point averages of CR averages of the CME rate (for widths greater than 30°) for lower cutoff speeds 200, 452 (average speed), 500, 600, 800, and 1000 km s^{-1}. The curve representing "All" corresponds to the CME rate of entire population. SSN (dashed) and SA (dotted) represent cotemporal sunspot number and area, respectively. Both SSN and SA are scaled down to fit suitably into the plot of CME rate. Tick marks on the top side horizontal axis represent the center date of the corresponding CR number shown in the bottom side horizontal axis. (b) The same as in (a) but for the entire population of CMEs without any distinction to their width. In this case the average speed is 426 km s^{-1}. Two horizontal dash-dotted lines labeled "1" and "2," represent respectively the mean levels of CME rate between CRs 2009 and 2071 for the entire population of CMEs and for the CMEs with cutoff speed greater than 200 km s^{-1}. This is to draw the attention of the reader toward the flat response of CME rate, instead of normal decline, during descending phase of the solar cycle.

distinction of width. Included are the Ra profiles for the entire population and the lower cutoff speeds of 200, 426 (average speed), 500, 600, 800, and 1000 km s^{-1}. Decrease in overall CME rate, by keeping the pattern of solar cycle variation intact for cutoff speeds greater than the average speed, by a factor of 2 is striking. This feature implies that the CMEs with speeds less than the average speed occur all through the solar cycle and contaminates the rate of CMEs of linear speeds greater than the average speed. Also the double-humped pattern becomes visibly more pronounced (Figure 2) for the CME rate with cutoff speeds greater than the average speed. The correlation of Rw (Ra) with SSN and SA is 0.933 (0.90) and 0.963 (0.95), respectively. The overall pattern of the variability of the CME rate seems to be similar to that of SA with the second peak larger than the first one in both the parameters. This feature persists in the rate of CMEs of any arbitrarily chosen cutoff speed (Figure 2) that is greater than the average speed. However, the

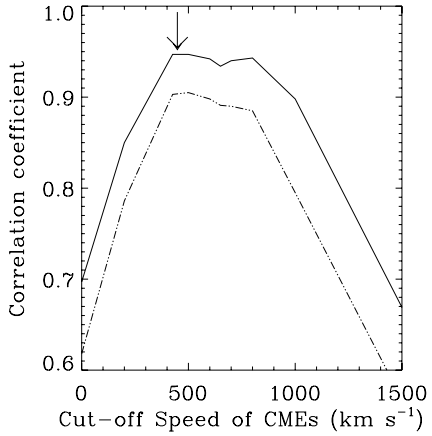

Figure 3. Correlation coefficient of CME rate vs. SA (continuous line) and SSN (dash-dotted line) for different cutoff speeds of CMEs. Note that the correlation is maximum (indicated by downward arrow) for the cutoff speed of 452 km s^{-1} (see the text for details).

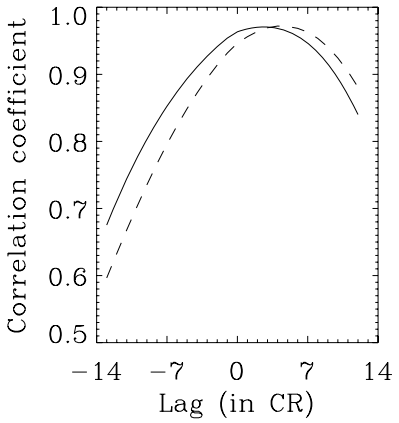

Figure 4. Correlation coefficient of the CME rate and the SA for different time lags. CME rate used here is for cutoff speed equal to the average speed for CMEs with width greater than 30° (continuous line) and for the entire population of CMEs (dashed line).

double-humped pattern with the dominant second peak slowly disappears with the increased cutoff speed beyond 1000 km s^{-1}. The two years' delay of CME rate with respect to the sunspot activity seems to be apparent only when the SSN index is considered (Gopalswamy et al. 2003; Kane 2006). Both SSN and SA indices are deduced from the same observed features (sunspots) on the visible disk of the Sun and yet show difference in their variability patterns with each one peaking at different times. Ramesh & Rohini (2008) have explained this difference as due to the same weight factor assigned to all the spot groups (g) while evaluating the number of spots for each day using the relation SSN $= k(10g + n)$, where k and n are the correction factor to bring all the observers to a common scale and the number of individual spots, respectively. It is, therefore, quite clear that the rate of CMEs, to a large extent, follows sunspot cycle, and that the maximum CME rate occurs in the same year as that of the maximum occurrence of SA but lags by two years when compared to SSN as is demonstrated here.

Since the sunspots occur in active regions, it is expected that the correlation between CME rate and solar activity is good only for those CMEs that originate from active regions. CMEs, however, are known to originate from filament regions. Our analysis (Figure 3) shows that the correlation between the CME rate and the sunspot activity (SA and SSN) maximize for CMEs with speeds greater than the average speed. Low correlation for cutoff speeds less than the average speed can be understood in terms of the contamination of CME rate with CMEs of speeds less than the average speed which occur in abundance (Gopalswamy et al. 2003; Mittal et al. 2009) and originate from locations outside of active regions (Song et al. 2007). Low correlation for the higher cutoff speeds (greater than the average speed) can be understood in terms of the scanty occurrence of CMEs with such higher speeds (Figure 2 of Gopalswamy et al. 2003). We may, therefore, infer that the CMEs with speeds greater than the average predominantly originate from the regions associated with sunspots. It also supports the view that the sunspot associated CMEs are energetic ones (Gopalswamy et al. 2009). This, however, does not completely rule out the possibility of contamination of sunspot associated CME rate with that of occasional filament associated high speed ones. Eventwise description of CMEs and the characteristics of their speed distribution with a critical assessment of their source regions would give better insight into the understanding of their overall variability.

Visual inspection of the crests and trough of the double-humped pattern of profiles of SA and CME rate (Figure 2) still indicate that the CME rate lags behind SA by about 6–8 rotations (about 7 months). Delay analysis (Figure 4), however, indicates that the overall CME rate (when all the three phases of the solar cycle are considered) lags behind SA by about five rotations when entire population of CMEs without any reference to the width (dashed curve) are considered and by about 2–3 rotations when CMEs with width more than 30° (continuous curve) are considered. Wheatland & Litvinenko (2001) have modeled the energy balance in the flaring corona and supported the view that the observed delay of about 6 months (overall delay over a period of solar cycle) between sunspot and flare numbers can be attributed to the hysteresis effect that can account for the coronal response time. Their model predictions however have shown a lag of about 11 months and explained the difference of 5 months between predicted and observed delays in terms of uncertainties in the data used for deriving the delay. Present lag analysis between CMEs and SA shows a broad peak around 2–3 months which is far less than the predicted coronal response time. Since the delay of three rotations is less than the averaging length (one year), we believe that the delay is most probably statistical than a true one. This small delay can also be attributed to the projection effects in deriving the speeds of CMEs particularly during the maximum phase of the solar cycle.

It is interesting to note that the CME rate and the SSN show a weak correlation during maximum phase of the solar cycle (Gopalswamy et al. 2009). This was explained in terms of the contamination of CME rate with the population of CMEs associated with high latitude quiescent filament regions. A scatter plot of CME rate (for CMEs with speeds greater than the average speed) against SA (Figure 5) indicates that it saturates for the mean SA greater than 1400 millionth of the solar hemisphere. We opine that this saturation effect might be one of the reasons for the mismatch, during solar maximum, between the CME rate and the sunspot activity though both of them show unambiguous double-humped pattern (Figure 2).

It is known that the CME productivity increases with active region size measured by SA (Canfield et al. 1999). Falconer et al. (2009) have reported that the active regions to produce CME or major flare, the nonpotentiality of their magnetic field should attain a threshold value and that, conversely, active regions, large or small, having nonpotentiality less than the threshold value are unlikely to produce a CME or major flare. SA, an approximate

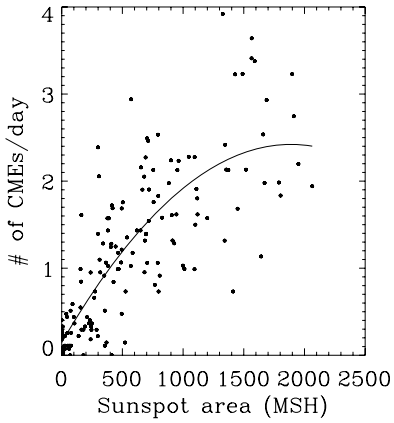

Figure 5. Scatter plot of the CME rate against daily SA (averaged over CR period), which shows saturation effect beyond 1400 MSH of SA. Earlier results (Gopalswamy et al. 2003) demonstrated a linear relationship between the CME rate and the SSN.

proxy for the flux content (assuming a uniform magnetic field all over the spot region), may attain large value but the development of nonpotentiality could be a delayed process. Usually, a single CME does not exhaust all the free energy in the active region. Therefore, during the lifetime of an active region (sometimes surviving for several rotations), magnetic field may attain threshold value of nonpotentiality several times and cause many CMEs. Saturation effect seen in Figure 5, therefore, indicates that the active region field attaining the nonpotentiality (Falconer et al. 2009) may play a dominant role over the flux content in producing CMEs. The origin of the magnetic twists, that may have strong bearing on the development of nonpotentiality, may come from the solar differential rotation, surface motions, and turbulent motions in the solar convection zone (Canfield & Pevtsov 2000). Therefore, the position (latitude) of the sunspot on the solar hemisphere may also play a role in causing a delay between the time of occurrence of CME and the time of maximum area of the spot. Such delays may cause a time lag between the CME rate and the SA (Figure 5) when overall correlations are considered over longer timescales. A study on the timescales of the development of maximum flux content and the development of nonpotentiality may give better insight into the observed lag of 2–3 months between the CME rate and the SA.

An eye-catching pattern of the CME rate is that during descending phase of the solar cycle it does not show a smooth decline (Figure 2(b)) to its minimum value just as SSN or SA does. Instead the CME rate shows a nearly flat response (at about 3.13 CMEs day^{-1} for entire population of CMEs and 2.44 CMEs day^{-1} for CMEs with cutoff speed greater than 200 km s^{-1}). This pattern is seen even when CMEs with angular size less than 30° are omitted (Figure 2(a)). However, the CME rate for the population with speeds greater than the average speed show more or less same pattern as that of SSN and SA (Figure 2). Smooth decline to its minimum values during descending phase for the rate of CMEs with speeds greater than the average speed may be due to the removal of contributions from low-speed ones which probably are associated with the quiescent prominences. This leads to an important conclusion that during declining phase of the solar cycle the loss of magnetic flux is through more frequent and less energetic CMEs though the solar cycle variability of CMEs is not completely void of high energetic events during descending phase. One such event is the cluster of CMEs and flares that occurred on 2005 September 15 associated with solar active regions NOAA AR 10808 (Liu et al. 2009). It will be quite interesting to see if this pattern repeats during descending phase of the ongoing solar cycle 24.

4. CONCLUSIONS

CMEs with speeds less than the average speed occur in all phases of the solar cycle and contaminate the CME rate with speeds greater than the average speed. CMEs with speeds greater than the average speed follow the sunspot cycle much better than the entire population of CMEs. Double-humped pattern during maximum phase is clearly seen in SSN, SA, flare rate, and in the CME rate as well. Comparison of the CME rate with SA does not show a delay of about two years in their peak occurrence while with SSN it is quite apparent. This reiterates the fact that the SA represents the solar cycle better than SSNs (Ramesh & Rohini 2008). Correlation coefficients between the rate of occurrence and SA maximize for CMEs with speeds greater than the average speed. The CME rate saturates for SA beyond 1400 millionths of the solar hemisphere. Also the peak occurrence of the CME rate lags behind the SA by about two–three months. We align with the view that the active region field attaining the nonpotentiality (Falconer et al. 2002), than the flux content as measured by the area of the active region, plays an important role in producing CMEs. During the declining phase of the solar cycle, the loss of magnetic flux is through more frequent and less energetic CMEs, probably through the prominence associated ones.

The author is grateful to Professors J. Hanumath Sastri and K. E. Rangarajan for their helpful suggestions and to the anonymous referee for suggestions that improved the contents of the Letter. The CME catalog is generated and maintained at the CDAW Data center by NASA and the Catholic University of America in cooperation with the Naval Research Laboratory. CACTus CME catalog is generated and maintained by the SIDC at the Royal Observatory of Belgium. *SOHO* is a project of international cooperation between ESA and NASA.

REFERENCES

Brueckner, G. E., et al. 1995, Sol. Phys., 162, 357
Canfield, R. C., Hudson, H. S., & McKenzie, D. 1999, Geophys. Res. Lett., 26, 627
Canfield, R. C., & Pevtsov, A. A. 2000, J. Astron. Astrophys., 21, 213
Cremades, H., & St. -Cyr, O. C. 2007, Adv. Space. Res., 40, 1042
Falconer, D. A., Moore, R. L., & Gary, G. A. 2002, ApJ, 569, 1016
Falconer, D. A., Moore, R. L., & Gary, G. A. 2009, ApJ, 700, L166
Gopalswamy, N., et al. 2003, in Solar Variability as an Input to the Earth's Environment, ed. A Wilson (Sp-535; Noordwijk: ESA), 403
Gopalswamy, N., et al. 2004, Adv. Space. Res., 34, 391
Gopalswamy, N., et al. 2005, J. Geophys. Res., A09S15, 110
Gopalswamy, N., et al. 2007, J. Geophys. Res., A06112, 112
Gopalswamy, N., et al. 2009, in Magnetic Coupling Between the Interior and Atmosphere of the Sun, ed. S. S. Hasan & R. J. Rutten (Berlin: Springer-Verlag), 289
Gosling, J. T., et al. 1976, Sol. Phys., 48, 389
Kane, R. P. 2006, Sol. Phys., 233, 107
Lippiello, E., de Arcangelis, L., & Godano, C. 2008, A&A, 488, L29
Liu, C., et al. 2009, ApJ, 703, 757
Low, B. C. 2001, J. Geophys. Res., 106, 25141
Mittal, N., et al. 2009, Planet. Space Sci., 57, 53
Ramesh, K. B., & Rohini, V. S. 2008, ApJ, 686, L41
Robbrecht, E., Berghmans, D., & Van der Linden, R. A. M. 2009, ApJ, 691, 1222
Sheeley, N. R., et al. 1999, J. Geophys. Res., 104, 24739
Song, W., Feng, X., & Hu, Y. 2007, ApJ, 667, L101
Wheatland, M. S., & Litvinenko, Y. E. 2001, ApJ, 557, 332
Yashiro, S., Michalek, G., & Gopalswamy, N. 2008, Ann. Geophys., 26, 3103